



Fatigue behavior of zirconia with microgrooved surfaces produced using femtosecond laser

Wenjin Li¹ · Qian Ding¹ · Fengbo Sun² · Binchao Liu³ · Fusong Yuan⁴ · Lei Zhang¹ · Rui Bao³ · Jinghua Gu⁵ · Yuanhua Lin²

Received: 2 May 2022 / Accepted: 19 November 2022

© The Author(s), under exclusive licence to Springer-Verlag London Ltd., part of Springer Nature 2023

Abstract

Femtosecond laser is a promising surface treatment tool for zirconia implant. In this study, the fatigue behavior of zirconia specimens with microgrooved surfaces formed by femtosecond laser is reported. One hundred sixty CAD/CAM zirconia bars (20 mm × 4 mm × 1.4 mm) were evenly divided into four groups with different surface: as sintered; sandblasted with 110 μm Al₂O₃; femtosecond laser produced microgrooves having 50 μm width, 30 μm depth, and 100 μm pitch; microgrooves having 30 μm width, 20 μm depth, and 60 μm pitch. The femtosecond laser formed micro/nanostructured microgrooves with precise size on zirconia surfaces. XRD analysis indicated that microgrooved surface showed no obvious tetragonal-to-monoclinic phase transformation. The fatigue strength of sandblasted specimens (728 MPa) was significantly higher than that of as sintered specimens (570 MPa). However, the fatigue strength of specimens with microgrooved surface decreased to about 360–380 MPa. The results suggest femtosecond laser is an effective technique to regulate the surface microtopography of zirconia, while further investigations are needed to improve its fatigue behavior.

Keywords Zirconia · Fatigue · Femtosecond laser · Microgrooves

✉ Lei Zhang
drzhanglei@yeah.net

¹ Department of Prosthodontics, Peking University School and Hospital of Stomatology, National Clinical Research Center for Oral Diseases, National Engineering Laboratory for Digital and Material Technology of Stomatology, Beijing Key Laboratory of Digital Stomatology, Beijing 100081, China

² School of Materials Science and Engineering, Tsinghua University, 100084 Beijing, China

³ School of Aeronautic Science and Engineering, Beihang University, 100191 Beijing, China

⁴ Center of Digital Dentistry, Peking University School and Hospital of Stomatology, National Clinical Research Center for Oral Diseases, National Engineering Laboratory for Digital and Material Technology of Stomatology, Beijing Key Laboratory of Digital Stomatology, Research Center of Engineering and Technology for Digital Dentistry, Ministry of Health, Beijing 100081, China

⁵ School of Materials Science and Engineering, Beihang University, Beijing 100191, China

Introduction

Yttria-stabilized tetragonal zirconia polycrystal (Y-TZP) is a promising alternative to titanium for producing dental implants [1]. It has excellent biocompatibility comparable to that of titanium [2]. In addition, compared to other stabilized-zirconia systems, 3Y-TZP has superior mechanical properties, including a high flexural strength (900–1100 MPa), fracture toughness (4.5–6 MPa/m²), and elastic modulus (200–210 GPa) [3, 4].

Zirconia implants have been subjected to many surface treatment methods, including sandblasting, acid etching, and coating, to improve osseointegration [5]. These procedures often require chemical solvents and introduce contaminants; moreover, they cannot precisely control surface micro-topography [6]. In recent years, femtosecond laser irradiation has been proved to be a viable zirconia surface microstructuring method. Femtosecond laser treatment is a noncontact, contaminant-free, and repeatable procedure, and it can be used to fabricate complex microstructure features with a high precision [7, 8]. The mechanism of femtosecond (10⁻¹⁵ s) laser ablation is ionization. Atoms under very short and intense pulses directly transform into plasma, thereby resulting in the removal of material without the melting,

evaporation, and solidification steps seen in nanosecond (10^{-9} s) or picosecond (10^{-12} s) laser fabrication processes [9]. The non-linear absorption of femtosecond laser can minimize thermal damage—even realize so-called cold ablation—and causes less collateral damage than conventional lasers such as Er: YAG and CO₂ lasers [10, 11]. The femtosecond laser can form micro-scale microgrooves on zirconia with nanostructures inside the microgrooves; this improves cell adhesion, migration, and proliferation [11]. Microgrooves enable the regulation of extracellular matrix orientation, and increase bone–implant contact and their mechanical interlocking [12, 13], which can be ascribed to “contact guidance.” Most previous studies have shown that microgrooves with 10–80 μm width and 3–50 μm depth are most favorable for osteoblast proliferation [11, 14–16]. The nanostructures enhance protein adsorption, osteoblast migration, and bone matrix formation [17].

Many studies have reported that microgrooved zirconia has excellent biological performance [18, 19]. However, unlike titanium, zirconia is a brittle material that can suddenly fracture without significant plastic deformation [20]. In addition, the mechanical strength of zirconia is reported to be sensitive to surface defects and structural flaws, and susceptible to fatigue under cyclic loading [21]. Surface treatments sometimes cause surface defects, leading to a decrease in the strength of the zirconia specimen. Moreover, the fracture origin in clinically failed zirconia implants was found to be directly related to surface defects formed by sandblasting, porous coatings, and machining [22, 23]. Microgrooves on the surface may also act as surface defects and decrease zirconia fatigue strength.

Mechanical strength is a crucial clinical consideration for zirconia implants. A retrospective clinical study reported that the first-generation zirconia implants had a 77.3% survival rate after 7 years of loading, and half of the failures were caused by implant fracture [24]. Although previous studies have mainly focused on the biocompatibility of laser-microgrooved zirconia, to the best of our knowledge, their mechanical strength and safety have no previous report and needed to be explored. To improve the biological performance with ensuring the mechanical performance, it's worthwhile to understand the effect of microgrooves on the mechanical performance of zirconia implants in detail. The purpose of our study was to demonstrate the fatigue behavior of zirconia bars with microgrooved surfaces produced using femtosecond laser. The dimensions of microgrooves were designed according to the results of previous studies that reported satisfactory osseointegration [15, 16].

Materials and methods

By following the ISO 6872:2015 guidelines for three-point flexural strength testing of ceramics, 160 bar-shaped specimens (20 mm × 4 mm × 1.4 mm) were produced.

Specimens were CAD/CAM milled from pre-sintered 3Y-TZP blocks (Zenostar T, Wieland, Germany) by using a cutting machine (Zenotec Mini, Wieland, Germany), followed by sintering in a high-temperature furnace (Ceramil Therm 3, Amann Girrbach). Edges of specimens were rounded to prevent stress concentration.

Laser surface treatment

A femtosecond fiber laser system (Tangerine, Amplitude Systems, France) (Fig. S1) was used for microstructuring. The laser pulse wavelength was 1030 nm, with a 400 fs pulse duration, 200 kHz repetition rate, and 1900 mm/s scanning speed. The average power of the system was 8 W. The pulse energy was 40 μJ. The specimen was fixed on a sample stage. The laser path (Fig. S2) was decided using a computer-controlled galvanometer. The microgroove size was adjusted by using lenses with different focal lengths and different numbers of passes.

Specimens were randomly and evenly divided into four groups according to the type of surface treatment as follows:

1. Sintered group (CTRL): there was no surface treatment after sintering, taken as control.
2. Sandblasted group (SB): the specimens were subjected to sandblasting using 110 μm alumina particles for 120 s with 0.4–0.5 MPa from a distance of 10–20 mm at an angle of 90° (Ovaljet HiBlaster, SHOFU, Japan). The sandblasting parameter in this study was the same as the parameter used for zirconia implants to achieve moderately rough surfaces (Ra between 1.0 and 2.0 μm) which is favorable for osseointegration [25].
3. Microgrooved group A (MG-A): microgrooves with 50 μm width, 30 μm depth, and 100 μm pitch were aligned perpendicular to the long axis of the specimen. The laser beam was focused by a lens with 175 mm focal length. The number of passes was 30.
4. Microgrooved group B (MG-B): a lens with 100 mm focal length was used to fabricate microgrooves with 30 μm width, 20 μm depth, and 60 μm pitch. The number of passes was 7.

Surface topography and roughness measurement

After surface treatment, specimens were cleaned in an ultrasonic bath with absolute alcohol and then with deionized water for 15 min each.

Specimens ($n = 2$) were subjected to platinum sputter-coating for microscopic observation with SEM (Merlin, Zeiss, Germany). All the specimens were scanned using a 3D laser

microscope (VK-9700 K, Keyence, Japan). The microgroove size of all the MG-A and MG-B specimens was determined by measuring the cross section profile of the microgrooves in the software package (VK analyzer, Keyence, Japan). Ten non-repetitive $50\ \mu\text{m} \times 50\ \mu\text{m}$ square areas without obvious defect were selected on each specimen to calculate surface roughness ($n=3$). The following surface roughness parameters were analyzed: Ra value (the arithmetic mean deviation of a profile), Rq value (the root-mean-square deviation of a profile), and Rz value (mean height of the irregularities at 10 points). The cross sections of microgrooves of two additional MG-A and MG-B specimens were characterized by SEM.

Surface wettability

The surface wettability was determined by measuring 1 μL droplet of double-distilled water within 10 s after application on three different locations of the specimen ($n=2$) using a contact-angle meter (OCA15Pro, Dataphysics, Filderstadt, Germany).

Phase analysis by X-ray diffraction

Specimens ($n=2$) were analyzed using an X-ray diffractometer (D/max 2500, Rigaku, Japan) to quantify the relative amount of the tetragonal phase to that of the monoclinic phase of the surface. Specimens were scanned with Cu K α , and spectra were collected in the 2θ range of 25° – 35° with a step interval of 1 s and step size of 0.02° . The monoclinic peak intensity ratio was obtained using the following equation [26]:

$$X_m = \frac{I_{m(111)} + I_{m(\bar{1}\bar{1}1)}}{I_{m(111)} + I_{m(\bar{1}\bar{1}1)} + I_{t(111)}} \quad (1)$$

where $I_{m(111)}$, $I_{m(\bar{1}\bar{1}1)}$, and $I_{t(111)}$ are the peak intensities around 31° , 28° , and 30° , respectively.

The monoclinic volume (V_m) was calculated using the following formula [27]:

$$V_m = \frac{1.311X_m}{0.311X_m + 1} \quad (2)$$

Flexural strength and fatigue strength test

Next, 20 specimens from each group were subjected to three-point flexural strength testing according to the ISO 6872:2015 Standard. Specimens were loaded on a Universal Testing Machine (AGS-X, Shimadzu, Japan) at a crosshead speed of 1 mm/min and with a loading span of 16 mm until failure. The flexural strength was calculated using the following equation:

$$\sigma_c = 3Fl/2wb^2 \quad (3)$$

where σ_c is the flexural strength, F is the fracture load (N), l is the span between support rollers (mm), w is the width of the specimen (mm), and b is the thickness of the specimen. Then, Weibull analysis was performed, and both the Weibull modulus m and characteristic strength σ_0 (the strength value at 63.21% failure probability) were calculated by the maximum likelihood estimation method (MATLAB R2014a) at a 95% confidence interval [28].

The setup used for the three-point flexural strength testing was also used to perform the fatigue test ($n=16$) using an electrical fatigue machine (ElectroPuls 1000, Instron, USA). Cyclic loading was applied at a frequency of 10 Hz for 10^6 cycles.

The cyclic fatigue strength in each group was determined by the staircase method. First, sinusoidal load ranging from the peak value, which was 60% of the fracture strength in the flexural test, to 10% of the peak value was applied to the specimens. The load increment was 5% of the peak value. If the specimen fractured, the load value that was one increment lower was applied to the next specimen. If the specimen survived, the load value that was one increment higher was applied to the next specimen. This procedure was continued until eight pairs of specimens with opposite results (fracture or survival) were observed. The fatigue strength limit (\hat{S}_m) and mean deviation ($\hat{\sigma}$) were determined using the following equation [29]:

$$\hat{S}_m = S_0 + d(A/N \pm 1/2) \quad (4)$$

$$\hat{\sigma} = 1.62 \times d((NB - A^2)/N^2 + 0.029) \quad (5)$$

if $(NB - A^2)/N^2 \geq 0.3$,

where S_0 is the lowest load value experienced by the less-frequent event, i.e., survival or failure; d is the load increment; and N is the total number of the less-frequent events ($\sum n_i$). The lowest stress level considered was designated as $i=0$, and so on until n_i , which was the number of failures or survivals at a given stress level. Further, $A = \sum in_i$ and $B = \sum i^2 n_i$. In Eq. (4), the positive sign is used if the least-frequent event is a survival.

Fractography examinations of two specimens from each group were conducted with SEM to determine the fatigue crack origin and fracture characteristics.

Statistical analysis

Descriptive statistics were computed. The assumption of normality was tested using the Shapiro–Wilk test. The homogeneity of variance was tested by performing the Levene test. Further, the surface roughness, contact angle,

flexural strength, and fatigue strength showed a nonparametric distribution, and the Kruskal–Wallis and pairwise comparison were used (SPSS 24.0; $\alpha = 0.05$).

Results

Surface topography and roughness

SEM images for all four groups are shown in Fig. 1. The CTRL group presented a relatively flat surface with a distinct grainy structure. SB surfaces exhibited scratches with sharp edges and irregular shapes. The MG-A and MG-B groups showed regularly aligned microgrooves without evident flaws, and the inner surface of the microgrooves was porous with nanoparticles. The size of the nanoparticles ranged from tens of nanometers to 300–500 nm. As in a previous study [18], this structure can be referred to as laser-induced periodic surface structure (LIPSS). The edges of the microgrooves were distinct without any collateral damage to the peripheral areas. The bottoms of microgrooves were “V” shaped (Fig. 2).

Fig. 1 SEM images of zirconia surface topographies

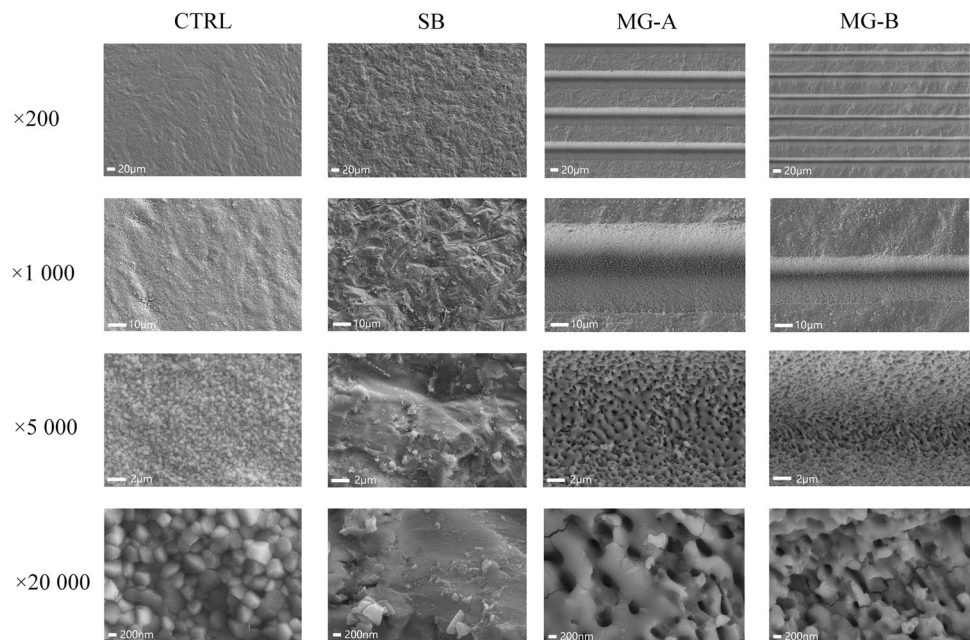
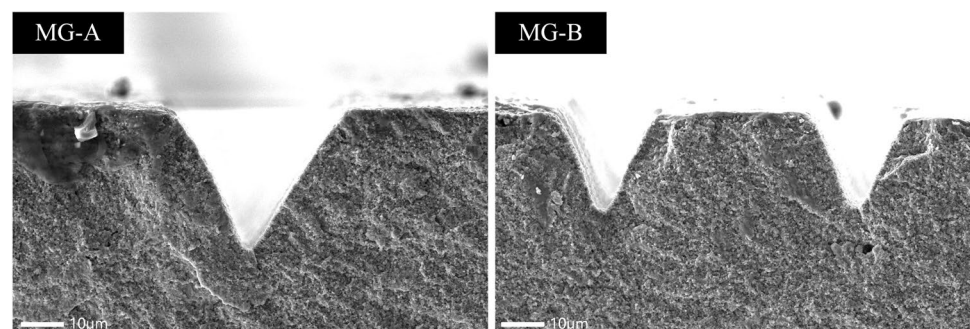


Fig. 2 SEM image of micro-grooved zirconia cross section. Magnification: 1000 \times . MG-A: microgrooves with 50 μm width, 30 μm depth, and 100 μm pitch. MG-B: microgrooves with 30 μm width, 20 μm depth, and 60 μm pitch



The surface roughness, as shown in Table 1, was in the following order: MG-A > MG-B > SB > CTRL. The precise microgroove dimensions, i.e., the width, depth, and pitch, are listed in Table 2.

Surface wettability

The surface wettability results are shown in Table 3. The contact angle of MG-B is statistically lower than MG-A ($p < 0.05$) and had no statistical difference with SB group ($p = 0.917$). The contact angle of MG-A is statistically higher than SB group ($p < 0.001$) and had no statistical difference with CTRL group ($p = 0.848$).

Phase transformation

XRD results (Fig. 3) showed no monoclinic phase peak in CTRL specimens, and the monoclinic phase content was 1.12%. An obvious monoclinic phase peak appeared

Table 1 Surface roughness of zirconia

Group	Ra (μm) Mean (SD)	Rq (μm) Mean (SD)	Rz (μm) Mean (SD)
CTRL	0.63 (0.09)a	0.81 (0.11)a	6.44 (0.92)a
SB	1.03 (0.12)b	1.29 (0.15)b	9.3 (1.30)b
MG-A	9.33 (0.47)c	10.58 (0.54)c	36.84 (2.32)c
MG-B	5.79 (0.83)d	6.77 (0.93)d	28.06 (3.11)d

The letters reflect the results of the Kruskal–Wallis test. Values with different letters were significantly different ($P < 0.001$).

Abbreviations: CTRL, sintered group; SB, sandblasted group; MG-A, microgrooves having 50 μm width, 30 μm depth, and 100 μm pitch; MG-B, microgrooves having 30 μm width, 20 μm depth, and 60 μm pitch.

Table 2 Dimensions of microgrooves

Group	Width (μm) Mean (SD)	Depth (μm) Mean (SD)	Pitch (μm) Mean (SD)
MG-A	48.84 (1.38)	30.81 (0.89)	100.38 (1.60)
MG-B	30.07 (0.99)	20.00 (1.35)	60.31 (0.84)

Table 3 Surface wettability of zirconia specimen

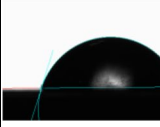
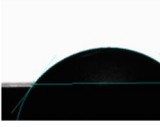
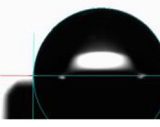
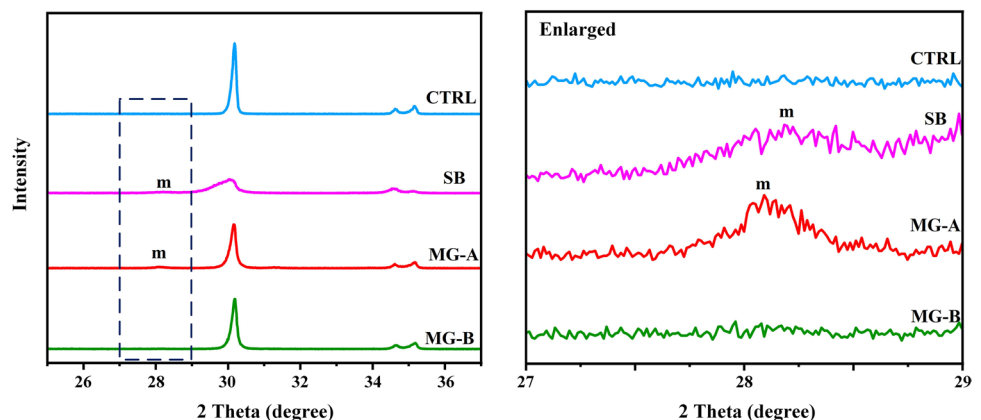
Group	CTRL	SB	MG-A	MG-B
Image				
Water contact angle ($^{\circ}$)	74.77 (1.16)	54.00 (1.28)	89.43 (1.59)	60.80 (3.71)

Fig. 3 X-ray diffraction spectra showing monoclinic-phase peak (m)

in SB, corresponding to a higher superficial monoclinic phase content of 16.09%. A slight monoclinic phase peak was observed for MG-A: the monoclinic phase content was 4.63%. The monoclinic phase peak was not detected for MG-B: the monoclinic phase content was 2.43%.

Flexural strength and fatigue strength

The flexural strength parameters are shown in Table 4. SB exhibited the highest flexural strength that was statistically similar to CTRL ($P = 0.446$). Further, the flexural strength of MG-A and MG-B was significantly lower than that of CTRL and SB ($P < 0.001$), but the difference in the flexural strength was not significant between MG-A and MG-B ($P = 0.131$). In addition, MG-A showed a higher Weibull modulus than did the other groups.

Fatigue strength data are presented in Table 4 and Fig. 4. The fatigue strength of MG-A and MG-B was similar ($P = 0.123$) but was significantly lower than that of the other two groups ($P < 0.005$). The fatigue

Table 4 Flexural strength parameters and fatigue strength

Group	Flexural strength (MPa) (σ_c) Mean (SD)	Fatigue strength (MPa) Mean (SD)	Characteristic strength (MPa) (σ_0)	95% CI	Weibull modulus (m)	95% CI
CTRL	903.54 (144.76)A	570.16 (25.47)a	964.84	901.53–1032.60	6.84	4.92–9.51
SB	979.26 (154.16)A	728.58 (35.54)b	1044.18	979.69–1112.91	7.27	5.18–10.21
MG-A	555.98 (35.74)B	384.95 (23.96)c	572.63	555.89–589.87	15.68	11.53–21.34
MG-B	505.20 (62.57)B	361.23 (13.11)c	533.07	503.05–564.87	8.04	5.91–10.93

The letters reflect the results of the Kruskal–Wallis test. Values with different letters were statistically different ($P < 0.005$)

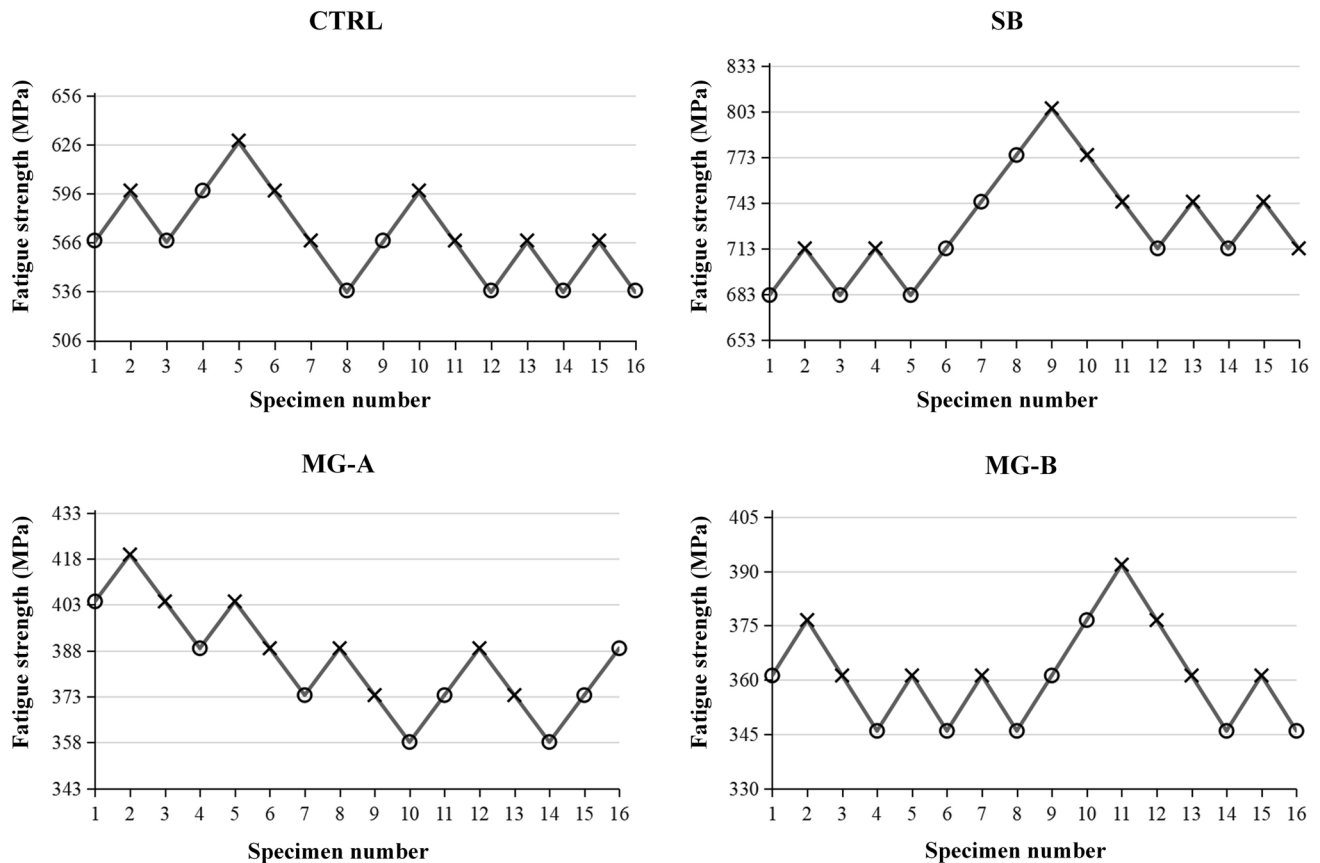


Fig. 4 Staircase plots obtained using fatigue test results for each group. The circle sign (O) indicates that the specimen survived, and the cross sign (X) indicates that the specimen fractured

strength of SB was statistically higher than that of CTRL ($P = 0.015$).

Fractography

Fatigue test results (Fig. 5) showed radial topographies representing crack propagation. The center of the radial lines are the fracture origins. The fracture origin was located at the surface defect formed due to processing or sandblasting in CTRL and SB. In two tested MG-A specimens, fractures started at the bottom of microgrooves. In one MG-B specimen, the

fracture origin was located at the bottom of a microgroove, while in another, the origin was located at the lateral wall of a microgroove.

Discussion

Lasers can produce microscale-to-nanoscale surface ripples with spatial frequency on almost all materials [30, 31], and the morphology depends on the material and laser parameters. The circular liquid rim surrounding the pores (Fig. 1)

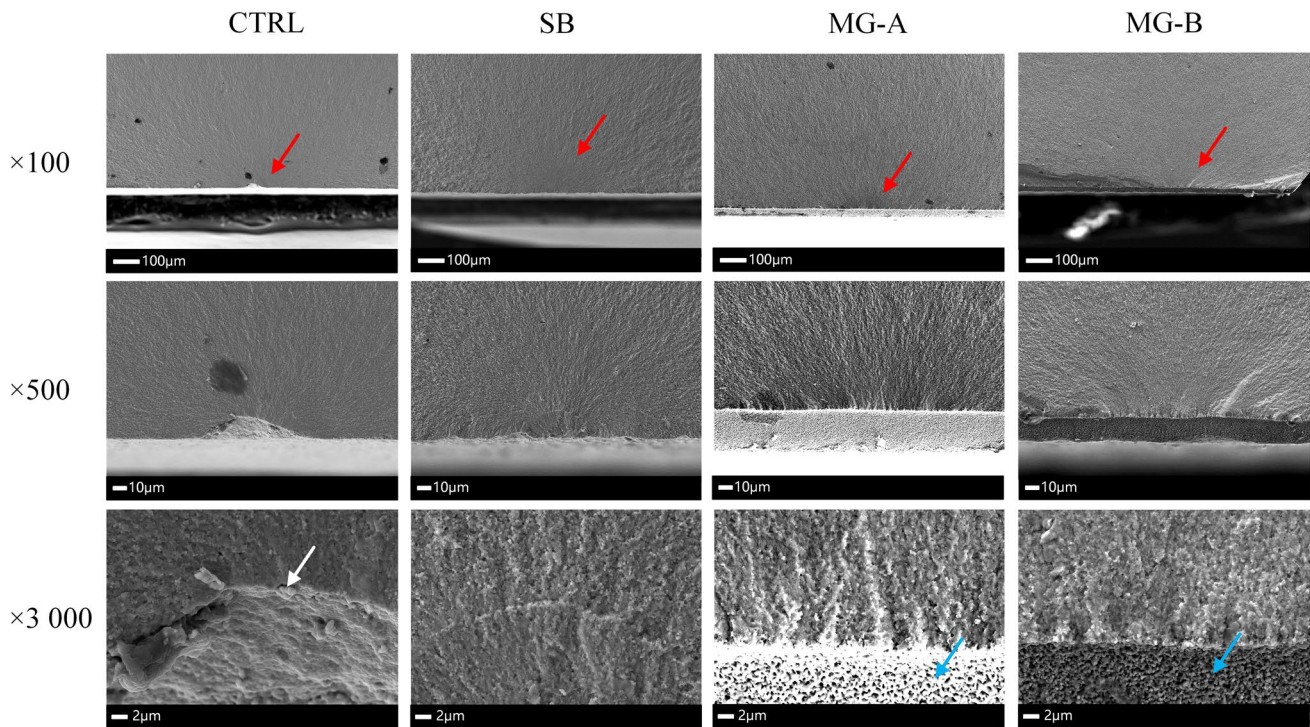


Fig. 5 SEM images of fatigue test fractography. Red arrows show the crack origin. Blue arrows show the lateral wall of microgrooves. The white arrow shows free-air-sintered grains. The fracture origin in

MG-A specimens was at the bottom of a microgroove. The fracture origin in MG-B specimens was on the lateral wall of a microgroove

was considered to indicate thermal melting. This phenomenon was related to the laser parameters used in this study. With a higher average laser power, the heat accumulation increases [32]. Further, a higher ablation efficiency results in a higher peak energy [33]. Therefore, further study is needed to optimize the processing parameters for zirconia surface treatment, i.e., to reduce the average power and increase the peak energy.

After sandblasting, the monoclinic phase content of the specimen increased to 16.09%, which was similar with that of the sandblasted zirconia implant (16.89%) using the same sandblasting method [25]. There was a slight monoclinic phase peak in MG-A with monoclinic phase content of 4.63%, which was not detected in MG-B with monoclinic phase content of 2.43%. This difference between the two microgrooved groups may be due to different laser parameters. Previous studies showed similar results: Delgado-Ruiz et al. [8] used femtosecond laser to fabricate grooves and pores on zirconia implants, and the monoclinic content tested by XRD was 1.72% and 1.94% respectively. Aivazi et al. [34] used a femtosecond laser to fabricate microgrooves on an alumina–zirconia nanocomposite specimen, and XRD results showed no tetragonal-to-monoclinic phase transformation after laser treatment. These previous reports were in accordance with the results of MG-B. Zhou et al. [35] discovered a slight increase in the monoclinic phase content of zirconia, and this was induced by laser ablation owing to the laser ablation time. So

the slight increase of monoclinic content in MG-A might be caused by relatively more scanning times.

The Weibull modulus m is a reference for the structural reliability of brittle dental materials. A higher Weibull modulus value shows lower variability and higher homogeneity, which can also be indicated by the standard deviation. Most dental ceramics have a Weibull modulus of 5–15 [36]. In this study, the size of microgrooves produced by the femtosecond laser had a high consistency, which led to a larger number of homogenous defects. Therefore, MG-A showed a high Weibull modulus. Zirconia specimens tended to fracture because of microgrooves rather than because of random defects, which can decrease the overall strength, despite the enhanced homogeneity.

The fracture of ceramic materials was believed to follow the “weakest link theory,” i.e., fracture is related to the largest flaw subjected to tensile stress [28]. The fatigue of zirconia is related to sub-critical crack growth (SCG). Any inherent defect can exhibit SCG when subjected to stresses and reaches a critical size, finally triggering catastrophic failure at a loading below the nominal strength of the material [37]. The flexural strength and fatigue strength of microgrooved zirconia are markedly lower than as sintered surface. The microgrooves acted as obvious stress concentrators. The stress concentration factor K_t of a notch can be calculated as follows [38]: $K_t = 1 + 2\sqrt{D/\rho}$, where D is the notch depth and

ρ is the root radius (defined at the point of minimum radius). Accordingly, microgrooves with a deeper and sharper bottom part experience higher stress concentration. Therefore, the microgrooves on the zirconia surface in this study led to a significant decrease in the strength. The fatigue strength of MG-B is slightly lower than MG-A. This is probably due to the higher aspect ratio (depth/width) and denser distribution of microgrooves that introduced more defects in MG-B.

The fatigue strength of SB was higher than that of CTRL. This possibly was the comprehensive impact of transformation toughening and surface defects. As is well known, under surface treatments like sandblasting, grinding, and machining, Y-TZP can experience stress-induced phase transformation [20]. Tetragonal-to-monoclinic phase transformation along with 3–4% volume expansion introduces a surface residual compressive layer that deters crack propagation and contributes to the strengthening of the Y-TZP material: this is referred to as “transformation toughening” [39]. Therefore, in many studies, sandblasting was adopted as an effective method to enhance the fatigue strength of 3Y-TZP implants and specimens [25, 40]. However, other studies reported that the defects produced by surface treatments can act as stress concentrators and reduce zirconia strength [41, 42]. In addition, it was reported [43] that abrasion with 50 μm alumina particles markedly reduced the fatigue strength of zirconia specimens from 1006.5 to 789.0 MPa. Moreover, the fatigue strength reduced to 307.5 MPa after abrasion with 120 μm alumina particles [43]. Chintapalli et al. [44] concluded that the particle size and pressure strongly affected the strength; when the defects extended beyond the compressive layer, they cannot be counteracted by the compressive stress field, and this finally decreases the zirconia strength. In this study, the transformation toughening effect of sandblasted zirconia might have negated the influence of defects, so the fatigue strength increased.

The fracture origins of specimens are different based on specific surfaces. Free-air-sintered grains were observed at the fracture origin of the CTRL group, which indicates that the defects were introduced before final sintering [45]. The fractures in the SB specimens initiated as a result of sintering- or sandblasting-induced defects, depending on the defect size. The fractures in the CTRL and SB groups were caused by random defects. The fracture origins of microgrooved zirconia were all concentrated inside the microgrooves, which further proved that microgrooves became dominant defects and raise higher concentration stress than random defects.

Conclusions

Within the limitations of this study, it can be concluded that the femtosecond laser can precisely and effectively form micro/nanostructured microgrooves on zirconia without

distinct phase transformation. Femtosecond laser is a promising surface treatment method for dental implant, which can realize selective microscopic topography regulation and has the potential to enhance osseointegration. However, microgrooves led to a significant decrease in the fatigue strength of zirconia. Further research is needed to enhance the mechanical strength of microgrooved zirconia by optimizing femtosecond laser parameters and the size of the microgrooves.

Supplementary information The online version contains supplementary material available at <https://doi.org/10.1007/s10103-022-03679-w>.

Acknowledgements The mechanical test in this work was done at the Dental Medical Devices Testing Center, Dental Materials Laboratory, Peking University School and Hospital of Stomatology, with the instruction from Dr. Gang Zheng and Wei Bai. The authors also give thanks to Dr. Jianqiao Zheng for the technical support during femtosecond laser surface treatment and Dr. Yuhan Liang for the help in XRD test.

Author contribution Conceptualization: Wenjin Li and Lei Zhang; methodology: Wenjin Li and Qian Ding; software: Binchao Liu; formal analysis: Rui Bao and Jinghua Gu; investigation: Wenjin Li and Fengbo Sun; resources: Fusong Yuan and Yuanhua Lin; data curation: Wenjin Li; writing—original draft preparation: Wenjin Li; writing—review and editing: Qian Ding and Lei Zhang; funding acquisition: Lei Zhang. All authors have read and agreed to the published version of the manuscript.

Funding This research was funded by the Natural Science Foundation of Beijing Municipality (Grant No. 7192233), the Capital Health Research and Development of Special (Grant No. 2020–2-4104), and the National Natural Science Foundation of China (Grant No. 81671026).

Data availability The data that support the findings of this study are available from the corresponding author, upon reasonable request.

Declarations

Conflict of interest The authors declare no competing interests.

Informed consent Not applicable because this research did not involve human participants.

References

1. Yoshinari M (2020) Future prospects of zirconia for oral implants -a review. *Dent Mater J* 39(1):37–45. <https://doi.org/10.4012/dmj.2019-151>
2. Kohal RJ, Weng D, Bachle M, Strub JR (2004) Loaded custom-made zirconia and titanium implants show similar osseointegration: an animal experiment. *J Periodontol* 75(9):1262–1268. <https://doi.org/10.1902/jop.2004.75.9.1262>
3. Zhang Y, Lawn BR (2018) Novel Zirconia Materials in Dentistry. *J Dent Res* 97(2):140–147. <https://doi.org/10.1177/0022034517737483>
4. Kailer A, Stephan M (2016) On the feasibility of the Chevron Notch Beam method to measure fracture toughness of fine-grained

- zirconia ceramics. *Dent Mater* 32(10):1256–1262. <https://doi.org/10.1016/j.dental.2016.07.011>
5. Schunemann FH, Galarraga-Vinueza ME, Magini R, Fredel M, Silva F, Souza JCM et al (2019) Zirconia surface modifications for implant dentistry. *Mater Sci Eng C Mater Biol Appl* 98:1294–1305. <https://doi.org/10.1016/j.msec.2019.01.062>
 6. Fischer J, Schott A, Martin S (2016) Surface micro-structuring of zirconia dental implants. *Clin Oral Implants Res* 27(2):162–166. <https://doi.org/10.1111/clr.12553>
 7. Duncan AC, Weisbuch F, Rouais F, Lazare S, Baquay C (2002) Laser microfabricated model surfaces for controlled cell growth. *Biosens Bioelectron* 17(5):413–426. [https://doi.org/10.1016/S0956-5663\(01\)00281-0](https://doi.org/10.1016/S0956-5663(01)00281-0)
 8. Delgado-Ruiz RA, Calvo-Guirado JL, Moreno P, Guardia J, Gomez-Moreno G, Mate-Sanchez JE et al (2011) Femtosecond laser microstructuring of zirconia dental implants. *J Biomed Mater Res B Appl Biomater* 96(1):91–100. <https://doi.org/10.1002/jbm.b.31743>
 9. Daskalova A, Bashir S, Husinsky W (2010) Morphology of ablation craters generated by ultra-short laser pulses in dentin surfaces: AFM and ESEM evaluation. *Appl Surf Sci* 257(3):1119–1124. <https://doi.org/10.1016/j.apsusc.2010.08.037>
 10. Stubinger S, Homann F, Etter C, Miskiewicz M, Wieland M, Sader R (2008) Effect of Er:YAG, CO₂ and diode laser irradiation on surface properties of zirconia endosseous dental implants. *Lasers Surg Med* 40(3):223–228. <https://doi.org/10.1002/lsm.20614>
 11. Carvalho A, Canguero L, Oliveira V, Vilar R, Fernandes MH, Monteiro FJ (2018) Femtosecond laser microstructured alumina toughened zirconia: a new strategy to improve osteogenic differentiation of hMSCs. *Appl Surf Sci* 435:1237–1245. <https://doi.org/10.1016/j.apsusc.2017.11.206>
 12. Ricci JL, Grew JC, Alexander H (2008) Connective-tissue responses to defined biomaterial surfaces I Growth of rat fibroblast and bone marrow cell colonies on microgrooved substrates. *J Biomed Mater Res A* 85(2):313–325. <https://doi.org/10.1002/jbm.a.31379>
 13. Khandaker M, Riahihezhad S, Williams WR, Wolf R (2017) Microgroove and collagen-poly(epsilon-caprolactone) nanofiber mesh coating improves the mechanical stability and osseointegration of titanium implants. *Nanomaterials (Basel)* 7(6):145. <https://doi.org/10.3390/nano7060145>
 14. Delgado-Ruiz RA, Gomez Moreno G, Aguilar-Salvatierra A, Markovic A, Mate-Sanchez JE, Calvo-Guirado JL (2016) Human fetal osteoblast behavior on zirconia dental implants and zirconia disks with microstructured surfaces. An experimental in vitro study. *Clin Oral Implants Res* 27(11):e144–e153. <https://doi.org/10.1111/clr.12585>
 15. Lee MH, Oh N, Lee SW, Leesungbok R, Kim SE, Yun YP et al (2010) Factors influencing osteoblast maturation on microgrooved titanium substrata. *Biomaterials* 31(14):3804–3815. <https://doi.org/10.1016/j.biomaterials.2010.01.117>
 16. De Luca AC, Zink M, Weidt A, Mayr SG, Markaki AE (2015) Effect of microgrooved surface topography on osteoblast maturation and protein adsorption. *J Biomed Mater Res A* 103(8):2689–2700. <https://doi.org/10.1002/jbm.a.35407>
 17. Souza JCM, Sordi MB, Kanazawa M, Ravindran S, Henriques B, Silva FS et al (2019) Nano-scale modification of titanium implant surfaces to enhance osseointegration. *Acta Biomater* 94:112–131. <https://doi.org/10.1016/j.actbio.2019.05.045>
 18. Rezaei NM, Hasegawa M, Ishijima M, Nakhaei K, Okubo T, Taniyama T et al (2018) Biological and osseointegration capabilities of hierarchically (meso-/micro-/nano-scale) roughened zirconia. *Int J Nanomedicine* 13:3381–3395. <https://doi.org/10.2147/IJN.S159955>
 19. Calvo-Guirado JL, Aguilar-Salvatierra A, Gomez-Moreno G, Guardia J, Delgado-Ruiz RA, de Val JEMS (2014) Histological, radiological and histomorphometric evaluation of immediate vs. non-immediate loading of a zirconia implant with surface treatment in a dog model. *Clin Oral Implan Res* 25(7):826–830. <https://doi.org/10.1111/clr.12145>
 20. Shen JZ, Kosmač T (2014) *Advanced ceramics for dentistry*. Elsevier, Amsterdam, p 78
 21. Zhang Y, Sailer I, Lawn BR (2013) Fatigue of dental ceramics. *J Dent* 41(12):1135–1147. <https://doi.org/10.1016/j.jdent.2013.10.007>
 22. Scherrer SS, Mekki M, Crottaz C, Gahlert M, Romelli E, Marger L et al (2019) Translational research on clinically failed zirconia implants. *Dent Mater* 35(2):368–388. <https://doi.org/10.1016/j.dental.2018.11.033>
 23. Osman RB, Ma SY, Duncan W, De Silva RK, Siddiqi A, Swain MV (2013) Fractured zirconia implants and related implant designs: scanning electron microscopy analysis. *Clin Oral Implan Res* 24(5):592–597. <https://doi.org/10.1111/j.1600-0501.2011.02411.x>
 24. Roehling S, Woelfler H, Hicklin S, Kniha H, Gahlert M (2016) A retrospective clinical study with regard to survival and success rates of zirconia implants up to and after 7 years of loading. *Clin Implant Dent Relat Res* 18(3):545–558. <https://doi.org/10.1111/cid.12323>
 25. Ding Q, Zhang L, Bao R, Zheng G, Sun YC, Xie QF (2018) Effects of different surface treatments on the cyclic fatigue strength of one-piece CAD/CAM zirconia implants. *J Mech Behav Biomed* 84:249–257. <https://doi.org/10.1016/j.jmbbm.2018.05.002>
 26. Garvie RC (1972) Phase analysis in zirconia systems. *J Am Ceram Soc* 55(6):303–305. <https://doi.org/10.1111/j.1151-2916.1972.tb11290.x>
 27. Toraya H, Yoshimura M, Somiya S (1984) Calibration curve for quantitative analysis of the monoclinic-tetragonal ZrO₂ system by X-ray diffraction. *J Am Ceram Soc* 67(6):C119–C121. <https://doi.org/10.1111/j.1151-2916.1984.tb19715.x>
 28. Quinn JB, Quinn GD (2010) A practical and systematic review of Weibull statistics for reporting strengths of dental materials. *Dent Mater* 26(2):135–147. <https://doi.org/10.1016/j.dental.2009.09.006>
 29. Collins JA (1993) *Failure of materials in mechanical design*. Wiley, New York
 30. Mezera M, Alamri S, Hendriks WAPM, Hertwig A, Elert AM, Bonse J et al (2020) Hierarchical Micro-/Nano-Structures on Polycarbonate via UV Pulsed Laser Processing. *Nanomaterials (Basel)* 10(6):1184. <https://doi.org/10.3390/nano10061184>
 31. Dufft D, Rosenfeld A, Das SK, Grunwald R, Bonse J (2009) Femtosecond laser-induced periodic surface structures revisited: a comparative study on ZnO. *J Appl Phys* 105(3):034908. <https://doi.org/10.1063/1.3074106>
 32. Weber R, Berger TGP, Onuseit V, Wiedenmann M, Freitag C, Feuer A (2014) Heat accumulation during pulsed laser materials processing. *Opt Express* 22(9):11312–11324. <https://doi.org/10.1364/OE.22.011312>
 33. Ulerich JP, Ionescu LC, Chen J, Soboyejo WO, Arnold CB (2007) Modifications of Ti-6Al-4V surfaces by direct-write laser machining of linear grooves. Conference on Photon Process Microelectronics Photonics. <https://doi.org/10.1117/12.713964>
 34. Aivazi M, Fathi MH, Nejatidanesh F, Mortazavi V, Hashemi Beni B, Matinlinna JP et al (2016) The evaluation of prepared micro-groove pattern by femtosecond laser on alumina-zirconia nanocomposite for endosseous dental implant application. *Laser Med Sci* 31(9):1837–1843. <https://doi.org/10.1007/s10103-016-2059-8>
 35. Zhou HB, Li C, Zhou ZK, Cao RY, Chen Y, Zhang SS et al (2018) Femtosecond laser-induced periodic surface microstructure on dental zirconia ceramic. *Mater Lett* 229:74–77. <https://doi.org/10.1016/j.matlet.2018.06.059>

36. Karakoca S, Yilmaz H (2009) Influence of surface treatments on surface roughness, phase transformation, and biaxial flexural strength of Y-TZP ceramics. *J Biomed Mater Res B* 91(2):930–937. <https://doi.org/10.1002/jbm.b.31477>
37. Gonzaga CC, Cesar PF, Miranda WG, Yoshimura HN (2011) Slow crack growth and reliability of dental ceramics. *Dent Mater* 27(4):394–406. <https://doi.org/10.1016/j.dental.2010.10.025>
38. Taylor D (2007) *The theory of critical distances: a new perspective in fracture mechanics*. Elsevier, Amsterdam, p 9
39. Piconi C, Maccauro G (1999) Zirconia as a ceramic biomaterial. *Biomaterials* 20(1):1–25. [https://doi.org/10.1016/s0142-9612\(98\)00010-6](https://doi.org/10.1016/s0142-9612(98)00010-6)
40. Amaral M, Cesar PF, Bottino MA, Lohbauer U, Valandro LF (2016) Fatigue behavior of Y-TZP ceramic after surface treatments. *J Mech Behav Biomed* 57:149–156. <https://doi.org/10.1016/j.jmbbm.2015.11.042>
41. Luthardt RG, Holzhter MS, Rudolph H, Herold V, Walter MH (2004) CAD/CAM-machining effects on Y-TZP zirconia. *Dent Mater* 20(7):655–662. <https://doi.org/10.1016/j.dental.2003.08.007>
42. Pereira GKR, Fraga S, Montagner AF, Soares FZM, Kleverlaan CJ, Valandro LF (2016) The effect of grinding on the mechanical behavior of Y-TZP ceramics: a systematic review and meta-analyses. *J Mech Behav Biomed* 63:417–442. <https://doi.org/10.1016/j.jmbbm.2016.06.028>
43. Aboushelib MN, Wang H, Kleverlaan CJ, Feilzer AJ (2016) Fatigue behavior of zirconia under different loading conditions. *Dent Mater* 32(7):915–920. <https://doi.org/10.1016/j.dental.2016.03.012>
44. Chintapalli RK, Marro FG, Jimenez-Pique E, Anglada M (2013) Phase transformation and subsurface damage in 3Y-TZP after sandblasting. *Dent Mater* 29(5):566–572. <https://doi.org/10.1016/j.dental.2013.03.005>
45. Scherrer SS, Lohbauer U, Della Bona A, Vichi A, Tholey MJ, Kelly JR et al (2017) ADM guidance—Ceramics: guidance to the use of fractography in failure analysis of brittle materials. *Dent Mater* 33(6):599–620. <https://doi.org/10.1016/j.dental.2017.03.004>

Publisher's note Springer Nature remains neutral with regard to jurisdictional claims in published maps and institutional affiliations.

Springer Nature or its licensor (e.g. a society or other partner) holds exclusive rights to this article under a publishing agreement with the author(s) or other rightsholder(s); author self-archiving of the accepted manuscript version of this article is solely governed by the terms of such publishing agreement and applicable law.